Silencing Sirtuin5 induces DNA damage by suppressing the pentose phosphate pathway in a demalonylation-dependent manner: A possible target for anticancer therapy in CRC

Hao-Lian Wang
Division of Gastroenterology and Hepatology; Key Laboratory of Gastroenterology and Hepatology, Ministry of Health; State Key Laboratory for Oncogenes and Related Genes

Yan Chen
State Key Laboratory for Oncogenes and Related Genes, Key Laboratory of Gastroenterology and Hepatology, Ministry of Health, Division of Gastroenterology and Hepatology, Shanghai Institute of Digest

Yun-Qian Wang
State Key Laboratory for Oncogenes and Related Genes, Key Laboratory of Gastroenterology and Hepatology, Ministry of Health, Division of Gastroenterology and Hepatology, Shanghai Institute of Digest

En-Wei Tao
State Key Laboratory for Oncogenes and Related Genes, Key Laboratory of Gastroenterology and Hepatology, Ministry of Health, Division of Gastroenterology and Hepatology, Shanghai Institute of Digest

Juan Tan
Division of Gastroenterology and Hepatology; Key Laboratory of Gastroenterology and Hepatology, Ministry of Health; State Key Laboratory for Oncogenes and Related Genes

Qian-Qian Liu
State Key Laboratory for Oncogenes and Related Genes, Key Laboratory of Gastroenterology and Hepatology, Ministry of Health, Division of Gastroenterology and Hepatology, Shanghai Institute of Digest

Chun-Min Li
State Key Laboratory for Oncogenes and Related Genes, Key Laboratory of Gastroenterology and Hepatology, Ministry of Health, Division of Gastroenterology and Hepatology, Shanghai Institute of Digest

Xuemei Tong
Department of Biochemistry and Molecular Cell Biology, Shanghai Jiao Tong University School of Medicine

Qin-Yan Gao
Division of Gastroenterology and Hepatology; Key Laboratory of Gastroenterology and Hepatology, Ministry of Health; State Key Laboratory for Oncogenes and Related Genes

Jie Hong
State Key Laboratory for Oncogenes and Related Genes, Key Laboratory of Gastroenterology & Hepatology, Ministry of Health

Ying-Xuan Chen (yingxuanchen71@sjtu.edu.cn)
State Key Laboratory for Oncogenes and Related Genes, Key Laboratory of Gastroenterology and Hepatology, Ministry of Health, Division of Gastroenterology and Hepatology, Shanghai Institute of Digest
https://orcid.org/0000-0002-1883-7736
Jingyuan Fang
State Key Laboratory for Oncogenes and Related Genes, Key Laboratory of Gastroenterology & Hepatology, Ministry of Health

---

Article

Keywords: Sirtuin5, DNA damage, anticancer therapy, colorectal cancer (CRC)

Posted Date: March 10th, 2021

DOI: https://doi.org/10.21203/rs.3.rs-276003/v1

Version of Record: A version of this preprint was published at Nature Communications on October 17th, 2022. See the published version at https://doi.org/10.1038/s41467-022-33903-8.

Abstract

A previous study by our research group showed that sirtuin5 (SIRT5), a member of the class III NAD -dependent deacetylase family, is highly expressed in colorectal cancer (CRC). The present study showed that deletion of SIRT5 induced cell cycle arrest and apoptosis as a result of continuous and irreparable DNA damage in CRC cells, a consequence of the impaired production of ribose-5-phosphate (R5P) which is essential for nucleotide synthesis. Consistently, the cell cycle arrest and apoptosis induced by SIRT5 silencing could be reversed by supplementation with four nucleotides. Moreover, metabolic profiling revealed that silencing of SIRT5 could inhibit the non-oxidative pentose phosphate pathway (PPP), which produces R5P, required for base ribosylation. Notably, SIRT5 activates transketolase (TKT), the key enzyme in the cellular non-oxidative PPP, by mediating its lysine demalonylation through the interaction between SIRT5 and TKT. Furthermore, the results demonstrated that TKT is essential for the SIRT5-induced malignant phenotypes of CRC, both in vivo and in vitro. These results therefore revealed that the increased lysine malonylation levels of TKT caused by silencing SIRT5 suppresses non-oxidative pentose phosphate metabolism, leading to a low-nucleotide pool. This in turn induces DNA damage in tumor cells and inhibits proliferation, suggesting that SIRT5 may serve as a potential anticancer target.

Introduction

Colorectal cancer (CRC) is a serious health problem in developed countries, with the second highest mortality rates worldwide[1].Cancer cells exhibit several malignant features and metabolic reprogramming is among the most important. During the development and progression of cancer, a series of metabolic enzymes are regulated by numerous post-translational modifications (PTM), including methylation, acetylation, succinylation, malonylation, glutarylation and glycosylation[2,3]. SIRT5 belongs to the family of nicotinamide adenine dinucleotide (NAD^+)-dependent class III histone deacetylase enzymes. It is located in both the mitochondria and cytosol and regulates a variety of metabolic pathways[4,5]. Additionally, SIRT5 was initially regarded as a deacetylase [6], although it was recently reported to have potent lysine demalonylase[4,7], desuccinylase[8,9] and deglutarylase[10,11] activity. Accumulating evidence also suggests that these non-canonical PTMs are involved in the regulation of cancer metabolic adaptations. Importantly, dysfunction of SIRT5 can cause a variety of diseases including cancer[12]. For example, a previous study showed that demalonylation and inactivation of SDHA by SIRT5 lead to the accumulation succinate, which activates thioredoxin reductase 2 (TrxR2) and confers resistance to chemotherapy[13]. Moreover, SIRT5 was shown to protect glutaminase (GLS) from ubiquitin-mediated degradation in a desuccinylation-dependent manner and leads to an increase in carbon and/or nitrogen, thus supporting the development of breast tumors[14]. Given that SIRT5 promotes the survival and proliferation of cancer cells in a context-specific manner[14–16], its role in metabolic reprogramming and tumor needs to be explored in detail.

Recent research demonstrated that an altered metabolism may affect genome stability by palying a role in DNA damage [17]. As it is known, integrity of the DNA structure is the basis for the viability of all living

cells and organisms, given that it is the main carrier of genetic information. Existing literature suggests that genomes may suffer from a variety of endogenous and exogenous DNA damaging factors, including replication errors, harmful chemical substances and various forms of ionizing radiation[18]. In the absence of prompt and correct DNA repair, cell senescence, cycle arrest and apoptosis may occur[19]. Tumor cells can adapt to changes in their microenvironment through metabolic reprogramming to refuel the pool of precursor molecules for lipid, nucleic acid and amino-acid synthesis[20].Among these, the pentose phosphate pathway (PPP) is an important source of R5P and nicotinamide adenine dinucleotide phosphate (NADPH) in the rapidly proliferating tumor cells. And R5P and NADPH are important precursors and hydrogen donors for DNA and RNA biosynthesis, respectively[21]. Furthermore, the PPP is composed of two branches, namely: an oxidation process, which can generate R5P, NADPH and CO_2 from glucose-6-phosphate and a non-oxidative process, which mainly converts the intermediate products of glycolysis, such as fructose-6-phosphate (F6P) and glyceraldehyde-3-phosphate (G3P), to R5P. Although R5P can be generated from the oxidative phase, more than 80% of R5P required for nucleotide synthesis in tumor cells is provided by the non-oxidative PPP[22]. To date, the transcriptional regulation of PPP mainly focuses on oncogenic mutations or alterations, such as the RAS, mTOR and NRF2[23–25]. However, the role of PTMs of the key enzymes in the non-oxidative PPP is limited. A previous study by our research group showed that SIRT5 was overexpressed in colorectal carcinoma tissues. Additionally, knockdown of SIRT5 in CRC cells could cause cell cycle arrest and apoptosis by regulating glutaminolysis as a result of suppressing GLUD1 activity in a glutarylation-dependent manner[26]. Nonetheless, little is currently known about the other mechanisms of action of SIRT5 at the cellular level.

In the present study, silencing SIRT5 was shown to induce DNA damage and activated the DNA damage response system in human CRC cells. In addition, knockdown of SIRT5 reduced the production of R5P by inhibiting the activity of the TKT enzyme through the non-oxidative PPP. Supplementation with four nucleotides could inhibit DNA damage. This therefore reversed the cell cycle arrest and apoptosis as well as inhibition of colony formation induced by silencing SIRT5. Mechanistically, the study demonstrated that SIRT5 enhances the activity of TKT by reducing its malonylation levels. This novel mechanism therefore provides new insights for the treatment of CRC.

Results

Silencing SIRT5 induced DNA damage in human CRC cells. A previous study by our research group showed that silencing SIRT5 induced cell cycle arrest and apoptosis in CRC cells[26]. In addition, stress-induced DNA damage was shown to cause cell cycle arrest and apoptosis[27]. Therefore, the present study examined whether silencing SIRT5 could induce DNA damage. The results revealed that γH2AX(Ser139), a marker of DNA damage, was up-regulated in the HCT116 and LoVo cells after treatment with two short interfering RNAs (siRNAs) targeting SIRT5, for 24, 36, 48 and 72h (Fig. 1a). Exposure of both cells lines to 50 μm of etoposide for 24 h was used as a positive control. Moreover, there was an increase in the γH2AX (Ser139) nuclear foci in both cell lines following deficiency of SIRT5 (Fig. 1b, c).The alkaline comet assay was then used to directly observe the effect of silencing SIRT5 on DNA damage. Consistently, there was a

significant increase in the tail moments after SIRT5 siRNAs transfection for 48h (Fig. 1d, e). Furthermore, eukaryotic cells usually activate ATM-Chk2 and/or ATR-Chk1 in response to stress-induced DNA damage, to arrest the cell cycle and initiate DNA repair[28]. Herein, there was an increase in the expression of p-ATM, p-ATR, p-CHK1 and p-CHK2 in the SIRT5 siRNA-treated HCT116 and LoVo cells, indicating that the DNA damage response (DDR) was simultaneously activated (Fig. 1f). In general, these results clearly showed that silencing SIRT5 could induce DNA damage and activate the DDR in human CRC cells.

SIRT5 sustained the nucleotide pool by enhancing the synthesis of R5P to maintain DNA stability. A decrease in the pool of nucleotides can lead to stalling in the replication fork of cancer cells and induce double-strand breaks[29]. In addition, it was previously reported that cancer cells utilized the reprogramming of PPP to replenish the pool of ribose-5-phosphate, which is the precursor for the biosynthesis of all types of nucleotides[21]. In order to examine whether SIRT5 had an effect on the reprogramming of metabolism in CRC, the study re-analyzed the previous GC-MS data of HCT116 cells treated with SIRT5 siRNA[30]. The metabolite set enrichment analysis showed that silencing SIRT5 caused significant changes in the PPP (Supplementary Fig. 1a), with a marked decrease in the levels of R5P and Ru5P (Fig. 2a and Supplementary Fig. 1b). Moreover, the downregulation of SIRT5 led to a decrease in the levels of purine nucleotides such as inosine monophosphate (IMP), adenosine monophosphate (AMP) and guanosine monophosphate (GMP). However, there was a negligible change in the levels of adenine and guanine, the basic components of purine nucleotides (Supplementary Fig. 1b), suggesting that the deficiency of purine nucleotides was mainly caused by the decrease in R5P. The results also revealed a decrease in the levels of pyrimidine nucleotides including uridine monophosphate (UMP) and cytidine monophosphate (CMP), in SIRT5-deficient HCT116 cells (Supplementary Fig. 1b). Interestingly, there was a 2-fold increase in the levels of carbamyl-aspartic acid (Supplementary Fig. 1b), indicating that the conversion of carbamyl aspartic acid to uridine monophosphate was blocked due to the deficiency of R5P. This in turn led to abnormalities in UMP and CMP synthesis in cells where SIRT5 was silenced. Furthermore, targeted metabolomic analysis for nucleotides confirmed that the nucleotide pool decreased when SIRT5 was downregulated (Fig. 2b). These results therefore suggested that inhibition of SIRT5 suppressed the PPP, thus impairing the production of R5P, needed for nucleotide synthesis.

Cancer cells lack enough nucleotides to maintain normal DNA replication and this leads to DNA damage. However, exogenous supplementation with nucleotides was shown to reduce DNA damage[31]. Conequently, the present study examined the effect of exogenous-nucleotide supplementation on DNA damage in the SIRT5 siRNA transfected CRC cells. As expected, exogenous supplementation with four nucleotides (A, U, C, G) reversed the DNA damage induced by the depletion of SIRT5, in a dose-dependent manner (Fig. 2c). Similarly, the supplementation of exogenous nucleotides led to a decrease in the number of γH2AX nuclear foci in both the HCT116 and LoVo cells where SIRT5 was knocked down (Fig. 2d, e). In addition, oxidative stress was reported to be one of the most common endogenous sources of DNA damage. Although the results showed that SIRT5 deficiency was accompanied by increased levels of reactive oxygen species (ROS), there was no change in the levels of 8-hydroxy-20-deoxyguanosine which is a marker of DNA oxidative damage (Supplementary Fig. 2). The results

therefore suggested that insufficient nucleotide synthesis rather than ROS, was the main cause of DNA damage induced by silencing SIRT5.

Additionally, cancer cells require an expansion of the nucleotide pool during the progression of the S-phase. The results showed that inhibition of SIRT5 expression reduced the levels of R5P which contributes to nucleotide metabolism and supplies precursors for DNA and RNA biosynthesis. We therefore speculated that suppression of SIRT5 might have a significant impact on DNA synthesis in tumor cells. Consequently, the 5-ethynyl-20-deoxyuridine (EdU) assay was performed on CRC cells after silencing SIRT5 to test this hypothesis. The findings showed that actively dividing CRC cells in the control group displayed bright and robust EdU fluorescence although depletion of SIRT5 led to a significant dimming of the EdU signal (Fig. 2f, g), suggesting the presence of impaired DNA synthesis following SIRT5 knockdown. Similar to immunofluorescence, flow cytometry analysis showed that silencing SIRT5 decreased the mean fluorescence intensity of the EdU^+ population (Fig. 2h, i). Moreover, the inhibition of DNA synthesis induced by SIRT5 knockdown was partially reversed by exogenously supplied nucleotides (Supplementary Fig. 1c).

Generally, these results indicated that the DNA damage and reduced DNA synthesis induced by suppression of SIRT5 in CRC cells was at least partially due to a low nucleotide pool.

Knockdown of SIRT5 induced cell cycle arrest and apoptosis in CRC cells by reducing the nucleotide pool. The study then examined whether the nucleotide pool might influence cell growth in human CRC cells. As a result, transfection of two short interfering RNAs in both cell lines significantly enhanced the proportion of cells in the G2/M and S phase as well as the level of apoptotic cells. However, supplementation with four exogenous nucleotides decreased the cell cycle arrest (Fig. 3a, b) and apoptosis (Fig. 3c, d) induced by DNA damage. Consistently, western blot analysis revealed that the expression of cyclin D1 and cyclin D3, two G1 phase regulators, was downregulated while the levels of cyclin E1 and cyclin A2 were upregulated in the HCT116 and LoVo cells transfected with SIRT5 siRNA. However, these effects were reversed after adding four nucleotides (Fig. 3e). In addition, the effects of suppressing SIRT5 and supplementing with four nucleotides, on apoptosis, were evidenced by the western blot analysis (Fig. 3e). Following this, the study performed soft agar colony formation assays and found that supplementation with four exogenous nucleotides significantly promoted anchorage-independent growth of HCT116 and LoVo cells (Fig. 3f, g). In general, these results suggested that the DNA damage induced by silencing SIRT5, might have resulted from an insufficient pool of nucleotides required to support the extensive proliferation of cancer cells.

SIRT5 promoted PPP by activating TKT in a deacylation-dependent manner. Glycolytic intermediates metabolize to R5P through the PPP, subsequently supporting base ribosylation and maintaining the nucleotide pool, which are required for DNA replication and cell growth. Given that PPP follows two metabolic pathways for the production of R5P, the study further used [1,2-$^{13}C_2$]-glucose as the tracer for isotopologue spectral analysis (ISA), to monitor which pathway mainly produced R5P in LoVo cells after SIRT5 knockdown. Figure 4a shows that R5P (M + 1) was produced by oxidative decarboxylation through

the oxidative PPP while R5P (M + 2) was generated through the non-oxidative route. In addition, there were increased levels of the R5P [M + 1] isotopologue derived from [1,2-$^{13}C_2$]-glucose and a significant reduction in flow through the non-oxidative PPP occurred in the cells where SIRT5 was depleted (Fig. 4b, c). These results therefore suggested that [1,2-$^{13}C_2$]-glucose was predominantly metabolized to R5P [M + 1] through the oxidative arm of the PPP due to blockage of the non-oxidative arm after SIRT5 knockdown.

Ribose-5-phosphate isomerase (RPI), ribulose-5-phosphate epimerase (RPE), transketolase (TKT) and transaldolase (TALDO) are four critical enzymes that regulate the production of R5P through the non-oxidative PPP (Fig. 4d). Therefore, in order to further explore the mechanism through which SIRT5 drives the non-oxidized PPP to produce R5P, the study explored these enzymes involved in non-oxidative PPP metabolism. Intriguingly, the western blot analysis revealed no significant changes in the protein levels of RPI, RPE, TKT and TALDO (Fig. 4e). Notably, SIRT5 was reported to be the post-translational modification enzyme that regulates the activities of metabolizing enzymes[12]. Therefore, the study speculated that SRIT5 might affect the activity of these enzymes then regulate metabolism in the non-oxidative PPP. To test this hypothesis, the localization of SIRT5 and the four enzyme was first studied using immunofluorescence. The results showed a strong co-localization between SIRT5 and TKT (Fig. 4f, g) but not with RPI, RPE and TALDO (Supplementary Fig. 3). Thereafter, the activity of TKT was assessed and the findings showed that knockdown of SIRT5 in HCT116 and LoVo cells resulted to marked inhibition of TKT activity, by 30% and 50%, respectively (Fig. 4h, i). Following this, the study constructed a control vector, an SIRT5 wild type (SIRT5 WT) and the H158Y mutant plasmid (SIRT5H158Y, a deacetylase inactive mutant without the lysine deacylation activity) and reintroduced the plasmids into the CRC cells. The results revealed a significant increased in TKT activity in cell lines overexpressing WT SIRT5 although there was no significant change in cells overexpressing the mutant and control plasmid vectors (Fig. 4j). These further confirmed that SIRT5 could activate TKT and this effect depended on its deacylation activity.

Thereafter the study used targeted metabolomics to assess the dNTP levels in the stable cell lines expressing the control vector, SIRT5 WT and the H158Y mutant plasmid. This was done to ascertain whether SIRT5 had an effect on the nucleotide pool owing to its catalytic activity. The results showed that the cells overexpressing SIRT5 WT had significantly increased dNTP levels (Fig. 4l), compared to the vector and SIRT5 H158Y transfected cells. Next, the different plasmid transfected cells were treated with a vehicle and 1μM Camptothecin (CPT), a DNA-damaging agent, for 2 h, respectively. They were then refreshed with a drug-free medium and incubated for an additional 6 h. As expected, there was a significant decrease in the levels of γH2AX in the SIRT5 WT cells, 6 h after the withdrawal of CPT. However, there was no significant change in the cells expressing the catalytic mutant of SIRT5 and the control vector (Fig. 4m). These results therefore suggested that ectopic expression of SIRT5 was favorable for the repair of double-strand breaks by regulating the dNTP pool in CRC cells, in a deacylation-dependent manner.

TKT played a role in the occurrence of an insufficient nucleotide pool and DNA damage induced by SIRT5 knockdown in CRC Cells. TKT, as a key enzyme in the non-oxidative PPP, provides more R5P to facilitate tumor proliferation and metastasis. Herein, the study tested whether TKT contributed to the production of precursors for nucleotide biosynthesis, mediated by SIRT5. The results showed that knockdown of TKT reversed the SIRT5-induced increase in the levels of dNTPs and NTPs in both HCT116 (Fig. 5a). Given that SIRT5 could regulate the activity of TKT and that inhibition of TKT activity reduced the production of dNTPs, the study further explored whether TKT played a role in the effect of SIRT5 on DNA synthesis. Consequently, ectopically expressed wild-type TKT and vector controls were transfected into the HCT116 and LoVo cells, followed by SIRT5 knockdown. The EdU assay showed that the decrease in DNA synthesis caused by SIRT5 knockdown was partially reversed by the overexpression of TKT (Fig. 5b, c). Moreover, the SIRT5-dependent inhibition of DNA damage induced by CPT was reversed following treatment with TKT siRNA (Fig. 5d). Similar results were observed in the cells treated with OT, which is an inhibitor of TKT activity (Fig. 5e). Furthermore, flow cytometry was conducted to determine whether TKT was required for the pro-proliferative effect of SIRT5. The findings showed that ectopic expression of TKT reversed the effects caused by the suppression of SIRT5 (Fig. 5f-i). In addition, the western blot analysis validated that the upregulation of apoptosis indicators, including cleaved caspase 3, cleaved caspase 8, cleaved caspase 9, cleaved PARP and the marker of DNA damage, γH2AX, after SIRT5 knockdown, was reversed following the ectopic expression of TKT (Fig. 5j). Therefore, these results suggested that SIRT5 knockdown resulted to an insufficient dNTP pool by regulating the activity of TKT then induced DNA damage, leading to inhibition of the proliferation of CRC cells.

SIRT5 activated TKT by mediating its demalonylation.

Given that a strong co-localization between SIRT5 and TKT was observed in the HCT116 and LoVo cells (Fig. 4f, g), the study explored whether the deacetylation activity of SIRT5 had an impact on their localization. As in Fig. 6a, b, the endogenously expressed TKT and FLAG-SIRT5 showed extensive co-localization and this localization was independent of the catalytic activity of SIRT5 because the SIRT5 mutant did not show impaired binding with TKT. The interaction between SIRT5 and TKT was further detected using the co-immunoprecipitation assay (Fig. 6c, d).

Since SIRT5 activated TKT dependent on its deacylation activity, it was hypothesized that the direct interaction between TKT and SIRT5 was favorable for the induction of the lysine deacylation of TKT. In a recent proteomic study[4], mouse TKT was detectably demalonylated by SIRT5 at 6 lysine residues. Therefore, the study first assessed the lysine malonylation levels of TKT upon SIRT5 treatment. The results revealed a significant decrease in the lysine malonylation levels of TKT in cells overexpressing the WT SIRT5 but not in CRC cells expressing the domain-negative (Fig. 6e). On the contrary, there was an increase in the malonylation levels of TKT in SIRT5-silenced HCT116 and LoVo cells (Fig. 6f). These findings therefore indicated that SIRT5 could affect the lysine malonylation levels of TKT. However, it was not clear whether TKT malonylation affected its enzyme activity. Since acyl-CoA could serve as the donor molecule for the lysine acylation modification[10], immunoprecipitated Hemagglutinin (HA)-tagged TKT

was incubated with malonyl-CoA. The results revealed a significant decrease in TKT activity, suggesting an inhibition of enzyme activity resulting from the malonylation of TKT (Fig. 6g-h).

Among the 6 malonylated sites on TKT, the malonylation level of lysine 281 was shown to change markedly in the absence of SIRT5[4].Lysine 281 is conserved in TKT orthologs from humans to *Gallus gallus*, indicating that this residue may be critical to some evolutionarily conserved function of TKT (Fig. 6i). As previously noted[32], malonylation shifts a lysine's charge by changing the positive charge of its ε-amino group to a negatively charged carboxylic acid. Therefore, in order to test whether modification of lysine 281 was sufficient to affect the enzymatic activity TKT, the study generated three mutated plasmids, substituting lysine (K) 281, K282, K283 with arginine (R) 281, R282, R283, respectively, where the latter retained a positive charge. Then HCT116 cells ectopically expressing wild-type TKT, the K281R, K282R, and K283R mutants, were treated with SIRT5 siRNAs. The malonylation level of TKT was then analyzed through western blotting. The findings showed that the K281R mutation resulted to a significant reduction in malonylation as shown in Fig. 6j. Moreover, suppression of SIRT5 increased the malonylation levels of wild-type TKT as well as the K282R and K283R mutants but not those of the K281R mutant, suggesting that TKT was malonylated in an SIRT5-lysine281-dependent manner (Fig. 6j). Consistently, the K281R TKT mutant did not respond to the SIRT5-mediated regulation of enzyme activity (Fig. 6k), indicating that lysine 281 in TKT is a major malonylation site of SIRT5. In general, these results suggested that ectopic expression of SIRT5 reduced the malonylation of TKT, subsequently leading to its activation.

The impact of TKT on SIRT5 mediated tumorigenesis in vivo

In order to ascertain the oncogenic role of TKT in SIRT5-mediated tumorigenesis *in vivo*, the study established a xenograft tumor model in nude mice with HCT116 cells, under different experimental conditions. The results showed that silencing SIRT5 resulted to a significant in decrease tumor volume and weight although these changes were blocked in cells stably expressing TKT *in vivo* (Fig. 7a-d). Expectedly, knockdown of SIRT5 dramatically increased the levels of γ-H2AX in xenograft tumors hence confirming the effect of SIRT5 on DNA damage. Nonetheless, this effect was reversed following the overexpression of TKT in the xenograft tumor tissues (Fig. 7E). Furthermore, the TUNEL assay revealed that there was an increase in tumor cell apoptosis following the knockdown of SIRT5 and overexpression of TKT was able to reverse this effect (Fig. 7f). Additionally, targeted metabolomic analysis of tumor lysates revealed that silencing SIRT5 resulted in a significant downregulation of Ru5P, R5P, dAMP and dUMP although overexpression of TKT reversed these changes (Fig. 7g). However, the amount of dNTPs was undectable since the intensity of the signal was not strong enough. Therefore, these results strongly supported the hypothesis that SIRT5 played an important role in CRC tumorigenesis by demalonylating and activating TKT, thus generating a sufficient nucleotide pool, required to support the proliferation of CRC cells.

Correlation between SIRT5 expression and γ-H2A.X expression in human CRC tissues

In order to further address the significance of DNA damage in SIRT5-mediated tumorigenesis at the clinical level, the study tested the correlation between the SIRT5 and γ-H2AX expression levels in 60 human CRC specimens. Immunohistochemistry of SIRT5 and γ-H2A.X revealed that high-expression of SIRT5 was significantly associated with low levels of γ-H2AX ($p < 0.001$) as shown in Fig. 7h. The results therefore demonstrated that the expression levels of SIRT5 were negatively correlated with the levels of γ-H2AX (Fig. 7i).

Discussion

Previous studies showed that SIRT5 was overexpressed in various types of cancer including CRC[26], hepatocellular carcinoma[33] as well as ovarian cancer[16] and was involved in the regulation of tumor cell survival and proliferation. The present study highlighted that silencing SIRT5 increased the lysine malonylation levels of TKT and this suppressed non-oxidative pentose phosphate metabolism, leading to insufficient supply of R5P for nucleotide synthesis. This in turn contributed to DNA damage in tumor cells and inhibited their growth (Fig. 8).

According to recent research, sirtuins including SIRT1[34,35], SIRT2[36], SIRT3[37], SIRT4[38], SIRT6[39,40] and SIRT7[41,42] maintain genomic integrity by directly deacetylating components of the DNA repair machinery or indirectly decreasing the production of ROS through metabolic reprogramming. However, the role of SIRT5 in regulating DNA damage remains largely unclear. Nonetheless, the present study provided evidence that knockdown of SIRT5 can cause DNA damage in CRC cells, tumor tissues from xenograft mouse models and human CRC specimens. It is widely known that DDR is a complex and orderly mechanism in cells that occurs in response to DNA damage[43]. Although the DDR systems including the ATM-CHK2 and ATR-CHK1 pathways were activated following the depletion of SIRT5, DNA damage persisted over time, indicating that harmful factors were still present.

Compelling evidence suggests that nucleotide deficiency can cause DNA damage due to stalling of the replication fork and production of mismatched DNA[31,44]. Given that SIRT5 regulates multiple cellular processes through metabolic reprogramming, the study speculated that SIRT5 might affect DNA damage by regulating the supply of nucleotides. The results showed that knockdown of SIRT5 could reduce the levels of R5P and the nucleotide pool in CRC cells. However, the DNA damage induced by silencing SIRT5 could be reversed by supplementation with four exogenous nucleotides (A, U, C, G). It was previously reported that unrepaired DNA damage induces cell apoptosis through the caspase-dependent apoptosis pathway[45]. In this study, the findings revealed that supplementation with exogenous nucleotides could inhibit the caspase activation induced by silencing SIRT5. Moreover, an abnormal pool of dNTP was shown to halt DNA replication during the S-phase[46]. Similarly, the present study revealed that addition of four nucleotides could reverse the cell cycle arrest induced by shortage of dNTPs, corroborating with previous studies which showed that the levels of dNTPs regulated the cell cycle by activating the DNA checkpoint[47,48]. Therefore, this study demonstrated that the role of SIRT5 in DNA damage, which was mainly exerted by maintaining the intracellular dNTP pool, finally affected the cell cycle and apoptosis.

In order to meet the high demand for nucleotides in tumor cells, the PPP becomes abnormally active, resulting to high levels of R5P[49]. A previous study revealed that approximately 80% of the R5P required for nucleotide synthesis is provided by the non-oxidative PPP in cancer cells[22], while normal cells generate R5P through the oxidative PPP. The findings from this study similarly revealed that silencing SIRT5 specifically inhibited the non-oxidative PPP, which is a metabolic characteristic of tumor cells, suggesting that it might be a potential therapeutic target. Moreover, TKT is the key enzyme in the non-oxidative PPP and controls the conversions between glycolysis and PPP. In rapidly proliferating tumor cells, TKT can covert the intermediate metabolites of glycolysis, including F6P and G3P, into R5P, for nucleotide synthesis. Furthermore, the expression of TKT can be increased at the transcriptional level to activate the non-oxidative PPP[25]. It is likely that this is not the only mechanism upregulating or activating TKT. Herein, the results showed that the activity of TKT was regulated by SIRT5 with post-translational modification. The results also showed that TKT was crucial for the SIRT5-mediated process of carcinogenesis, both *in vivo* and *in vitro*. In addition, it was reported that TKT was able to counteract oxidative stress by supplementing NADPH and this was beneficial to cancer growth[50]. This may partly explain why silencing SIRT5 increased the levels of ROS in CRC cells.

Moreover, reversible malonylation of lysines is involved in numerous metabolic processes, including glycolysis, gluconeogenesis, the urea cycle and fatty acid β-oxidation[4]. However, it is still unclear how lysine demalonylation affects PPP. The results obtained in this study revealed an interaction between SIRT5 and TKT, leading to the demalonylation of K281, subsequently activating TKT in CRC. A previous study also showed that TKT phosphorylation affects its enzyme activity in human cervical cancer cells [51]. However, malonylation is likely to have a more profound effect on protein structure and function compared to other modifications due to its negatively charged nature and the large size of modification[4,52]. Collectively, these findings provide more insights on the role of malonylation in the regulation of PPP which is critical for cellular DNA integrity and survival. Nonetheless, further studies are needed to elucidate the specific mechanisms.

In conclusion, the present study showed that SIRT5 regulates non-oxidative PPP by activating TKT in a demalonylation-dependent manner, thereby increasing the generation of R5P required for nucleotide synthesis. This in turn affects DNA damage and cell proliferation in CRC. Additionally, this study provides a better understanding of the close interaction between SIRT5, cell metabolism and DNA damage. More importantly, the results identify SIRT5 as a potential target for CRC treatment.

Methods

Cell culture. The human CRC cell lines HCT116 and LoVo were obtained from the ATCC (the American Type Culture Collection, Manassas, VA, USA) and maintained at 37°C in a humidified incubator containing 5% CO2, in McCoy's 5A (Gibco BRL, Grand Island, NY, USA) supplemented with 10% Fetal Bovine Serum (FBS; Gibco BRL) and a Penicillin-Streptomycin Solution. The cell lines were free of *Mycoplasma*. The following chemicals were also added into the culture media used in this study: Campathecin(catalog

#CSN16581) and the TKT inhibitor, Oxythiamine (catalog #136-16-3) were purchased from CSNpharm (Chicago, USA) while Adenosine (catalog # 58-61-7); Guanosine (catalog #118-00-3); Cytidine (catalog #65-46-3) and Uridine (catalog #58-96-8) were bought from Sangon Biotech (Shanghai, China).

SiRNA transfection. The siRNAs specifically targeting SIRT5 has been described previously. The SIRT5 siRNAs comprised of the following sequences: siRNA-1, 5'- GCUGGAGGUUAUUGGAGAATT – 3', siRNA-2, 5'- GUGGCUGAGAAUUACAAGATT – 3'. In addition, the siRNA specifically targeting TKT was purchased from GenePharma (Shanghai, China). The TKT siRNA included: 1) 5'- CCAGCCAACAGCCAUCAUUTT – 3', 2) 5'- CCGGCAAAUACUUCGACAATT – 3'.

These siRNAs were transfected into subconfluent cells using the Dharma FECT 1 transfection reagent (Dharmacon, Lafayette, CO, USA) according to the manufacturer's instructions.
Each transfection was conducted in six-well plates where 30% confluent CRC cells were transfected with 1μg of small interfering RNA (siRNA) and 5μL of Dharma FECT 1 in 100 μL of the Opti-MEM medium (Invitrogen). The negative control was a nonspecific siRNA (NC-siRNA).

Western blotting. Cells or tissues were collected and lysed using the Radioimmunoprecipitation Assay (RIPA) lysis buffer supplemented with a protease inhibitor cocktail (Kangcheng, Shanghai, China). Proteins were then separated through SDS-polyacrylamide Gel Electrophoresis (SDS-PAGE) before being immunoblotted. The following primary antibodies were used: anti-SIRT5 (catalog #HPA022002, 1:2000, Sigma-Aldrich), anti-γ-H2A.X (catalog #9718, 1:1000), anti-p-ATM (catalog #5883, 1:1000), anti-p-ATR (catalog #2853, 1:1000), anti-p-CHK1 (catalog #2348, 1:1000), anti-p-CHK2 (catalog #2197, 1:1000), anti-cleaved caspase 3 (catalog #9664, 1:1000), anti-cleaved caspase 8 (catalog #9496, 1:1000), anti-cleaved caspase 9 (catalog #7237, 1:1000), anti-cleaved PARP (catalog #5625, 1:1000), anti-cyclin D1 (catalog #2978, 1:1000), anti-cyclin D3 (catalog #2936, 1:1000), anti-cyclin A2 (catalog #4656, 1:1000), anti-cyclin E1 (catalog #20808, 1:1000) and anti-α-tublin (catalog #2148, 1:2000) were purchased from Cell Signaling Technology (Danvers, MA, USA); anti-ATM (catalog #70103, 1:1000), anti-ATR (catalog #70109, 1:1000), anti-TKT (catalog #101477, 1:1000) and anti-TALDO1 (catalog# 102076, 1:1000), which were purchased from GeneTex (California, TX, USA). On the other hand, anti-CHK1 (catalog #8048, 1:1000), anti-CHK2 (catalog #5278, 1:1000) anti-RPI (catalog #515328, 1:1000) and anti-RPE (catalog #393655, 1:1000) were purchased from Santa Cruz Biotechnology, (Santa Cruz, CA, USA) while anti-FLAG (catalog #F1804, 1:1000, Sigma-Aldrich); anti-HA (catalog #MMS-101P, 1:1000, Convance, Princeton, NJ, USA); anti-pan succinylation (catalog #PTM-401,1:1000), anti-pan glutarylation (catalog #PTM-1151, 1:2000) and anti-pan malonylation (catalog #PTM-901, 1:1000) were obtained from PTM Biolabs (HangZhou, China). The secondary antibodies included; the Anti-beta Actin antibody (catalog #KC-5A08, 1:2000, Kang Cheng, China), Peroxidase-conjugated anti-rabbit antibody and anti-mouse antibodies (1:5000, Kangcheng). Thereafter, the western blot bands were detected using an ECL western blotting substrate (Thermo Scientific, Waltham, MA, USA) and the analysis was repeated at least three times.

Assessment of the cell cycle and apoptosis. Progression of the cell cycle and apoptosis were analyzed through flow cytometry. Briefly, the HCT116 and LoVo cells were cultured under the specified conditions.

In the cell cycle assay, cells were stained with 50 μg/mL of propidium iodide containing 20 μg/mL RNase (DNase-free) after which they were analyzed using flow cytometry according to the manufacturer's instructions. The G1, S (DNA synthesis phase), G2 and M (mitosis) phases were then identified based on the content of DNA and the study obtained the percentage of cells in the distinct phases. All the experiments were performed at least three times. Analysis was also conducted using an FITC Annexin V fluorescein isothiocyanate (FITC)/propidium iodide (PI) double stain assay (BD Pharmingen, San Diego, CA, USA). The stained cells were then analyzed through flow cytometry.

EdU Uptake.

Half of the medium was replaced with a fresh medium containing 20 μM of EdU for 2 h followed by fixation in 3.7% formaldehyde in PBS then a 0.5% TritonX-100 permeabilization step.
500 μL of the Click-iT reaction cocktail was used per coverslip, according to the manufacturer's protocol (Click-iT EdU Iamge kits, Life Technologies, catalog no. C10338). Thereafter, the hoechst 33342 dye was bound to DNA and the average fluorescence intensity was quantified using the Zeiss digital image processing software, ZEN® (blue edition). In the EdU Flow Cytometry Assay, EdU was detected using Pacific Blue™ azide at an excitation of 405 nm in a violet emission filter (Click-iT EdU Flow Cytometry Assay Kits, Life Technologies, catalog no. C10418). The percentage of EdU^+ cells was then analyzed using the FlowJo software.

The Soft Agar Colony Formation Assay. The soft agar colony formation assay was conducted 48 h after transfection with the SIRT5 siRNA. The cells were counted and seeded in six-well plates at 10^4 cells in a layer of 0.7% agar/complete growth medium over a layer of 1.2% agar/complete growth medium in the wells of a 6-well plate. Then, a cell medium containing the indicated concentration of four nucleotides (A, U, C, G) was replenished every 3 days. Cultures were grown in a humidified incubator at 37°C. 21 days after seeding, the cells were incubated with 4% paraformaldehyde for 10 min and 0.5% crystal violet was used to stain the colonies. Thereafter, megascopic colonies were quantified under a light microscope. Colonies, whose diameter was larger than 50 μm were counted and analyzed.

Measurements of enzyme activity. The cells were homogenized with ice-cold 0.1 M Tris-HCl buffer (pH 7.6) and centrifuged at 12000 rpm for 15 min after which the supernatant was collected. The protein concentration was then determined using the BCA Protein Assay Kit and recorded as C (g/L). Then, TKT activity was measured as previously described by Bayoumi and Rosalki, with minor modifications. Briefly, the supernatant (50 μL) was mixed with a 200 μL reaction mixture containing 14.4 mmol/L ribose-5-phosphate, 190 μM/L NADH, 380 μM/L TPP, > 250 U/L glycerol-3-phosphate dehydrogenase and > 6500 U/L triose phosphate isomerase. The Optical Density (OD) of TKT was then measured immediately at 340 nm, then once every 5 min for 1h. Moreover, TKT activity was deduced from the difference in absorbance measured at 15 and 45 min. The enzyme activity assay was repeated three times for each group. The TKT activities (%) of the treated group were then normalized to those of the control category (100%).

Immunofluorescence. The HCT116 or LoVo cells were plated in 4-well chamber slides and transfected with siRNA or plasmids as indicated. Forty-eight hours after transfection, cells were fixed with 4% formaldehyde, permeabilized with 0.2% Triton X-100 and blocked in 1% BSA in PBS for 1 h at room temperature. The cells were then stained using rabbit polyclonal anti-γH2A.X (1:400), rabbit polyclonal anti-TKT (1:100), rabbit polyclonal anti-TALDO1 (1:100), mouse monoclonal anti-RPI (1:100), mouse monoclonal anti-RPE (1:100), mouse monoclonal anti-FLAG (1:1200), rabbit polyclonal anti-SIRT5(1:100, Sigma) and mouse polyclonal anti-SIRT5(1:100, Santa Cruz) antibodies followed by secondary antibodies (donkey anti-mouse Dylight 488 and donkey anti-rabbit Dylight 594), respectively. Thereafter, fluorescence was analyzed using a confocal laser scanning microscope (Carl Zeiss, AG, Germany). After staining with DAPI (1:10,000), the media chamber was removed from the glass slide, which was treated using the Prolong Gold antifade reagent (P7481) and sealed with a coverslip. 24 h later, the average fluorescence intensity was quantified using the Zeiss digital image processing software, ZEN® (blue edition). Finally, co-localization analysis was performed using the “colocalization” module of the ImageJ program.

The Comet Assay. The HCT116 and LoVo cells were transfected with SIRT5 or negative control siRNA. DNA damage was then measured using the comet assay (single-cell gel electrophoresis) 48 h after transfection, where the comet assay kit (Cell Biolab, San Diego, CA, USA) was used according to the manufacturer’s instructions. Biefly, the cells (1 x 10^5 cells/mL) were re-suspended in ice-cold PBS (without Mg^{2+} and Ca^{2+}). Thereafter, the cell samples were mixed with Comet Agarose at a ratio of 1:10 (v/v), homogenized by pipetting then the mixture (75 µL/well) was transferred immediately onto the OxiSelect™ Comet Slide. The slide was maintained horizontally and carefully transferred from the alkaline solution to a horizontal electrophoresis chamber. Electrophoresis was then run in an alkaline buffer. Notably, the assay was performed under low/dim light conditions to avoid damage to the cell samples by ultraviolet light. Following this, the slides were viewed through epifluorescence microscopy using a FITC filter. In addition, measurement was done using a public domain PC-image analysis programme CASP software, version 1.2.2 (CASPLab, University of Wroclaw, Wroclaw, Poland). The comet assay was repeated at least three times and the tail moment was calculated.

Immunohistochemistry (IHC). Tumors dissected from nude mouse xenograft models of CRC were subjected to IHC to detect γH2AX and SIRT5. Sections (3 mm-thick) were incubated with the antibodies against γH2AX (1:400; CST) and SIRT5 (1:400, Sigma). HRP-conjugated secondary antibodies were used and subsequently mounted with Diaminobenzidine (DAB). Pathological evaluation was then conducted in a blinded manner. Moreover, apoptosis was detected using the Terminal Deoxynulceotidyl Transferase Nick-end-labeling (TUNEL) staining Kit (Keygen Biotech, Nanjing, China) according to the manufacturer’s instructions.

In vivo**models.** For the rescue-function experiments, nude mice (nu/nu, male, 5 weeks old) were weighed and injected subcutaneously with HCT116 cells (2 × 10^6 cells). Thereafter, the mice were randomly divided into four groups, including the control vector or TKT WT with or without SIRT5 knockdown. Then, two adenoviruses targeting the SIRT5 and TKT genes were used every 3 days. Moreover, the diameters of

the tumors were measured every 3 days using calipers. Additionally, the tumor volumes were calculated using the formula: (shortest diameter)^2 × (longest diameter) × 0.5. The tumors were eventually dissected and analyzed.

All animal studies were conducted according to the guidelines published by the Animal Ethics Committee of Renji Hospital, Shanghai Jiao Tong University, School of Medicine.

Measurement of Metabolite Levels.

For stable isotope-tracing analysis, LoVo cells (2 × 10^6/sample) were grown to 80% confluence in complete media. The cells were briefly rinsed twice with PBS then the medium was replaced with DMEM (glucose-free) supplemented with 11.11 mM [1,2-$^{13}C_2$]-glucose, 2 mM label-free glutamine in 10% dialyzed FBS, 100 units mL^{-1} Penicillin-Streptomycin and 3.7g/L sodium bicarbonate for 0.5h, 1h, 6h, 12h and 24h. Thereafter, the cell metabolites were extracted by adding pre-cold 80% (vol/vol) methanol and centrifuged at 15000g for 15 minutes, at 4 ℃. The supernatant was evaporated until it became dry. The residues were then reconstituted in 100 µL of 50% aqueous acetonitrile (1:1, v/v) prior to UHPLC-HRMS/MS analysis. Additionally, chromatographic separation was performed on a ThermoFisher Ultimate 3000 UHPLC system with a Waters BEH Amide column (2.1mm × 100 mm, 1.7 µm). The injection volume was 2 mL, the flow rate was 0.4 mL/min and the column temperature was 10℃. The mobile phases consisted of water (phase A) and acetonitrile/water (90:10, v/v) (phase B), both with 15mM ammonium acetate (pH = 9, modified by ammonium hydroxide). Moreover, a linear gradient elution was performed using the following program: 0 min, 95% B and held to 2 min; 5 min, 85% B; 7 min, 80% B; 11 min, 75%B; 12 min, 55% B and held to 13.5 min; 14 min, 95% B and held to 18 min. Thereafter, the eluents were analyzed separately using a ThermoFisher Q Exactive™ Hybrid Quadrupole-Orbitrap™ Mass Spectrometry (QE) in a Heated Electrospray Ionization Negative (HESI-) mode. For stable isotope-tracing analysis, the measured distribution of mass isotopomers was corrected for the natural abundance of isotopes using the IsoCor software.

Finally, the study used Liquid Chromatography Tandem Mass Spectrometry (LC-MS/MS) techniques, for targeted metabolomic analysis. A standard curve for the (d)NTP standard was prepared and used to determine the concentration of (d)NTPs in each unknown sample.

Statistical analysis. Data are shown as the means ± standard deviation (SD). Comparisons of data between two groups were performed using Student's t-test (two-tailed). For multiple comparisons, an analysis of variance (ANOVA) test was used. The correlation between the expression of SIRT5 and TKT was analyzed using the χ2-test. *P* values < 0.05 was accepted as statistically significant.

Declarations

Competing interests:

The authors declare no competing financial interests.

Author contributions

H.-L.W. and Y.-X.C. designed the experiments, analyzed the data, and wrote the

Acknowledgments

This study was supported by the National Natural Science Foundation of China (No. 81972203, 81772506, 81530072, 81830081, 8190236), the Shanghai Shenkang Center (SHDC12018121) and the Shanghai Municipal Education Commission-Gaofeng Clinical Medicine Grant Support (No. 20152210).

References

1. Bray, F. et al. Global cancer statistics 2018: GLOBOCAN estimates of incidence and mortality worldwide for 36 cancers in 185 countries. *CA Cancer J. Clin.***68**, 394–424, (2018).
2. Carrico, C., Meyer, J. G., He, W., Gibson, B. W. & Verdin, E. The Mitochondrial Acylome Emerges: Proteomics, Regulation by Sirtuins, and Metabolic and Disease Implications. *Cell Metab.***27**, 497–512, (2018).
3. Campbell, S. L. & Wellen, K. E. Metabolic Signaling to the Nucleus in Cancer. *Mol. Cell.***71**, 398–408, (2018).
4. Nishida, Y. et al. SIRT5 Regulates both Cytosolic and Mitochondrial Protein Malonylation with Glycolysis as a Major Target. *Mol. Cell***59**, 321–332, (2015).
5. Zhu, S. et al. The roles of sirtuins family in cell metabolism during tumor development. *Semin. Cancer. Biol.***57**, 59–71, (2019).
6. Nakagawa, T., Lomb, D. J., Haigis, M. C. & Guarente, L. SIRT5 Deacetylates carbamoyl phosphate synthetase 1 and regulates the urea cycle. *Cell***137**, 560–570, (2009).
7. Du, J. et al. Sirt5 is a NAD-dependent protein lysine demalonylase and desuccinylase. *Science***334**, 806–809 (2011).
8. Rardin, M. J. et al. SIRT5 regulates the mitochondrial lysine succinylome and metabolic networks. *Cell Metab.***18**, 920–933, (2013).
9. Wang, G. et al. Regulation of UCP1 and Mitochondrial Metabolism in Brown Adipose Tissue by Reversible Succinylation. *Mol. Cell***74**, 844 (2019).
10. Tan, M. et al. Lysine glutarylation is a protein posttranslational modification regulated by SIRT5. *Cell Metab.***19**, 605–617, (2014).
11. Zhou, L. et al. SIRT5 promotes IDH2 desuccinylation and G6PD deglutarylation to enhance cellular antioxidant defense. *EMBO Rep.***17**, 811–822, (2016).
12. Bringman-Rodenbarger, L. R., Guo, A. H., Lyssiotis, C. A. & Lombard, D. B. Emerging Roles for SIRT5 in Metabolism and Cancer. *Antioxid. Redox. Sign.***28**, 677–690, (2018).
13. Du, Z. et al. Targeting a Sirt5-Positive Subpopulation Overcomes Multidrug Resistance in Wild-Type Kras Colorectal Carcinomas. *Cell Rep.***23**, 3975–3978, (2018).

14. Greene KS, L. M., Wang X, Blank B, Druso JE, Lin MJ, Stalnecker CA, Zhang C, Negrón Abril Y, Erickson JW, Wilson KF, Lin H, Weiss RS, Cerione RA. SIRT5 stabilizes mitochondrial glutaminaseand supports breast cancer tumorigenesis. *Proc. Natl Acad. Sci. USA***116**, 26625–26632, (2019).
15. Ma, Y. et al. SIRT5-mediated SDHA desuccinylation promotes clear cell renal cell carcinoma tumorigenesis. *Free. Radic. Biol. Med.***134**, 458–467, (2019).
16. Sun, X. et al. SIRT5 Promotes Cisplatin Resistance in Ovarian Cancer by Suppressing DNA Damage in a ROS-Dependent Manner via Regulation of the Nrf2/HO-1 Pathway. *Front. Oncol.***9**, 754, (2019).
17. Li, M. et al. Transketolase Deficiency Protects the Liver from DNA Damage by Increasing Levels of Ribose 5-Phosphate and Nucleotides. *Cancer. Res.***79**, 3689–3701, (2019).
18. Zeman, M. K. & Cimprich, K. A. Causes and consequences of replication stress. *Nat. Cell Biol.***16**, 2–9, (2014).
19. Roos, W. P., Thomas, A. D. & Kaina, B. DNA damage and the balance between survival and death in cancer biology. *Nat. Rev. Cancer.***16**, 20–33, (2016).
20. Boroughs, L. K. & DeBerardinis, R. J. Metabolic pathways promoting cancer cell survival and growth. *Nat. Cell Biol.***17**, 351–359, (2015).
21. Patra, K. C. & Hay, N. The pentose phosphate pathway and cancer. *Trends. Biochem Sci.***39**, 347–354, (2014).
22. Boros, L. G. et al. Oxythiamine and dehydroepiandrosterone inhibit the nonoxidative synthesis of ribose and tumor cell proliferation. *Cancer. Res.***57**, 4242–4248 (1997).
23. Ying, H. Q. et al. Oncogenic Kras Maintains Pancreatic Tumors through Regulation of Anabolic Glucose Metabolism. *Cell***149**, 656–670, (2012).
24. Duvel, K. et al. Activation of a metabolic gene regulatory network downstream of mTOR complex 1. *Mol. Cell***39**, 171–183, (2010).
25. Mitsuishi, Y. et al. Nrf2 redirects glucose and glutamine into anabolic pathways in metabolic reprogramming. *Cancer cell***22**, 66–79, (2012).
26. Wang, Y. Q. et al. Sirtuin5 contributes to colorectal carcinogenesis by enhancing glutaminolysis in a deglutarylation-dependent manner. *Nat. Commun.***9**, 545, (2018).
27. Hafner, A., Bulyk, M. L., Jambhekar, A. & Lahav, G. The multiple mechanisms that regulate p53 activity and cell fate. *Nat Rev Mol Cell Biol***20**, 199–210, (2019).
28. Reinhardt, H. C., Aslanian, A. S., Lees, J. A. & Yaffe, M. B. p53-deficient cells rely on ATM- and ATR-mediated checkpoint signaling through the p38MAPK/MK2 pathway for survival after DNA damage. *Cancer cell***11**, 175–189, (2007).
29. Petermann, E., Orta, M. L., Issaeva, N., Schultz, N. & Helleday, T. Hydroxyurea-stalled replication forks become progressively inactivated and require two different RAD51-mediated pathways for restart and repair. *Mol. Cell***37**, 492–502, (2010).
30. Xia, J., Sinelnikov, I. V., Han, B. & Wishart, D. S. MetaboAnalyst 3.0–making metabolomics more meaningful. *Nucleic Acids. Res.***43**, W251-257, (2015).

31. Bester, A. C. et al. Nucleotide deficiency promotes genomic instability in early stages of cancer development. *Cell***145**, 435–446, (2011).
32. Peng, C. et al. The first identification of lysine malonylation substrates and its regulatory enzyme. *Mol.Cell. Proteomics.***10**, M111 012658, (2011).
33. Zhang, R. et al. SIRT5 Promotes Hepatocellular Carcinoma Progression by Regulating Mitochondrial Apoptosis. *J. Cancer.***10**, 3871–3882, (2019).
34. Wang, R. H. et al. Impaired DNA damage response, genome instability, and tumorigenesis in SIRT1 mutant mice. *Cancer cell***14**, 312–323, (2008).
35. Liu, T. et al. A divergent role of the SIRT1-TopBP1 axis in regulating metabolic checkpoint and DNA damage checkpoint. *Mol. Cell***56**, 681–695, (2014).
36. Zhang, H. et al. ATRIP Deacetylation by SIRT2 Drives ATR Checkpoint Activation by Promoting Binding to RPA-ssDNA. *Cell Rep.***14**, 1435–1447, (2016).
37. Liu, J. et al. SIRT3 protects hepatocytes from oxidative injury by enhancing ROS scavenging and mitochondrial integrity. *Cell. Death. Dis.***8**, e3158, 2017.564 (2017).
38. Jeong, S. M. et al. SIRT4 has tumor-suppressive activity and regulates the cellular metabolic response to DNA damage by inhibiting mitochondrial glutamine metabolism. *Cancer cell***23**, 450–463, (2013).
39. Cea, M. et al. Evidence for a role of the histone deacetylase SIRT6 in DNA damage response of multiple myeloma cells. *Blood***127**, 1138–1150, (2016).
40. Tian, X. et al. SIRT6 Is Responsible for More Efficient DNA Double-Strand Break Repair in Long-Lived Species. *Cell***177**, 622–638 e622, (2019).
41. Li, L. et al. SIRT7 is a histone desuccinylase that functionally links to chromatin compaction and genome stability. *Nat. Commun.***7**, 12235, (2016).
42. Tang, M. et al. SIRT7-mediated ATM deacetylation is essential for its deactivation and DNA damage repair. *Sci. Adv.***5**, eaav1118, (2019).
43. O'Connor, M. J. Targeting the DNA Damage Response in Cancer. *Mol. Cell***60**, 547–560, (2015).
44. Williams, L. N. *et al.* dNTP pool levels modulate mutator phenotypes of error-prone DNA polymerase epsilon variants. *Proc. Natl Acad. Sci. USA***112**, E2457-2466, (2015).
45. Surova, O. & Zhivotovsky, B. Various modes of cell death induced by DNA damage. *Oncogene***32**, 3789–3797, (2013).
46. Pajalunga, D. et al. A defective dNTP pool hinders DNA replication in cell cycle-reactivated terminally differentiated muscle cells. *Cell. Death. Differ.***24**, 774–784, (2017).
47. Pai, C. C. et al. Set2 Methyltransferase Facilitates DNA Replication and Promotes Genotoxic Stress Responses through MBF-Dependent Transcription. *Cell Rep.***20**, 2693–2705, (2017).
48. Pfister, S. X. et al. Inhibiting WEE1 Selectively Kills Histone H3K36me3-Deficient Cancers by dNTP Starvation. *Cancer cell***28**, 557–568, (2015).

49. Jiang, P. et al. p53 regulates biosynthesis through direct inactivation of glucose-6-phosphate dehydrogenase. *Nat. Cell Biol.***13**, 310–316, (2011).
50. Xu, I. M.-J. et al. Transketolase counteracts oxidative stress to drive cancer development. *Proc. Natl Acad. Sci. USA***113**, E725-E734, (2016).
51. Saha, A. et al. Akt phosphorylation and regulation of transketolase is a nodal point for amino acid control of purine synthesis. *Mol. Cell***55**, 264–276, (2014).
52. Hirschey, M. D. & Zhao, Y. Metabolic Regulation by Lysine Malonylation, Succinylation, and Glutarylation. *Mol.Cell. Proteomics.***14**, 2308–2315, (2015).

Figures

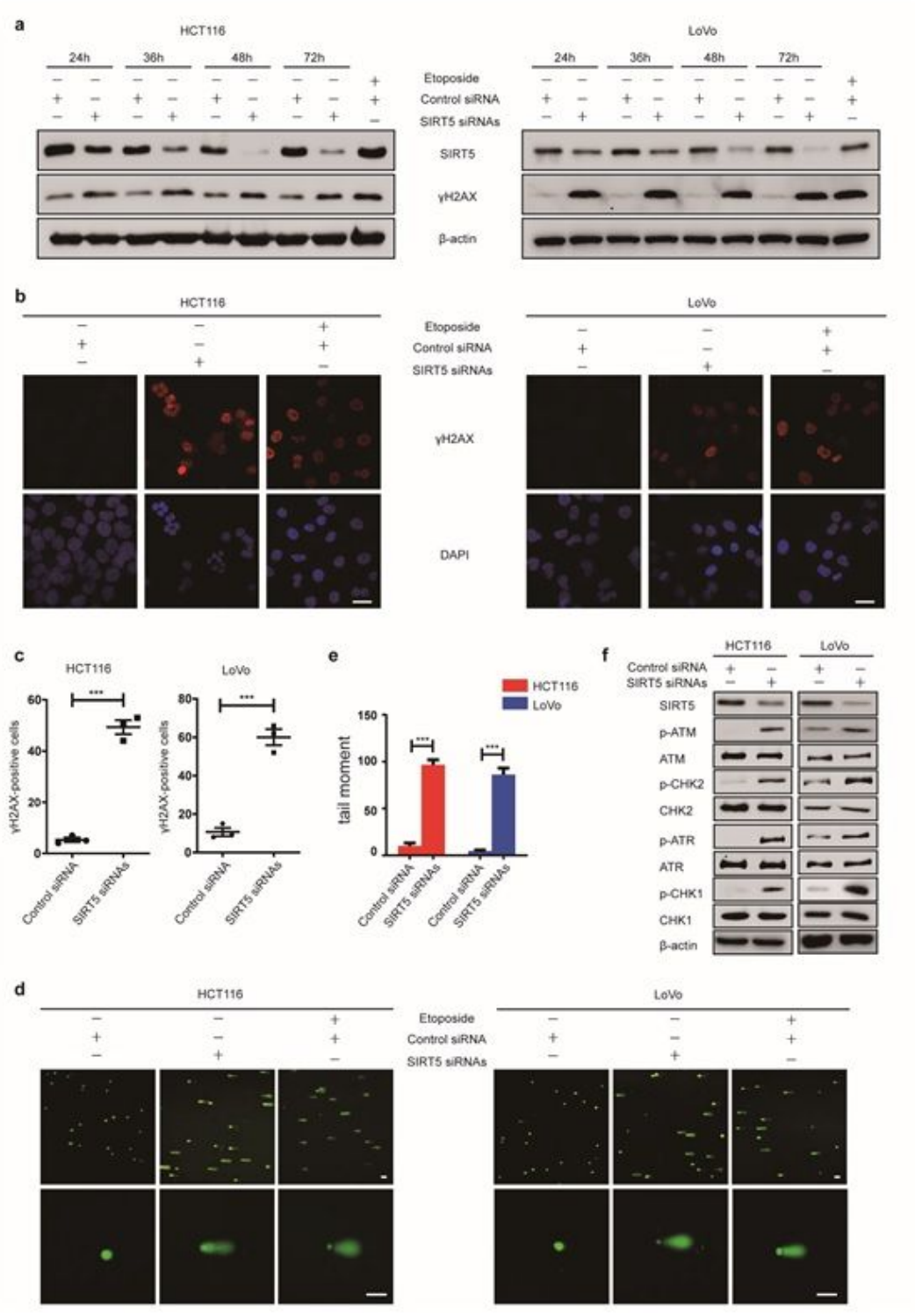

Figure 1

Silencing SIRT5 induced DNA damage. a Effect of SIRT5 on the γH2AX (Ser139) levels. Etoposide was applied as a positive control. Representative western blot images of the negative control or SIRT5 siRNAs-transfected HCT116 (left) and LoVo (right) cells after 24, 36, 48, or 72h. b, c Knockdown of SIRT5 caused the formation of γH2AX (Ser139) nuclear foci. Representative images (b) and quantification through immunofluorescence staining (c) for γH2AX (Ser139) in HCT116 (left) and LoVo (right) cells for 48h.

Etoposide was used as a positive control. The percentage of positive cells (>10 foci) out of 100 cells for each sample was calculated and plotted. The scale bars indicate 20 μm. d, e Effect of SIRT5 on DNA damage using the comet assay. Representative images of three independent experiments after 48h of SIRT5 siRNAs transfection in the HCT116 and LoVo cells (d). Scale bars indicate 20 μm. The extent of DNA damage was determined by measuring the tail moment for 100 individual comets. Data was quantified and graphed (e). f Representative western blots showing that the DDR pathway was activated in CRC cells after depletion of SIRT5. β-actin was used as the loading control. Results in C and E were presented as mean ± SD from three independent samples. ***p 0.001.

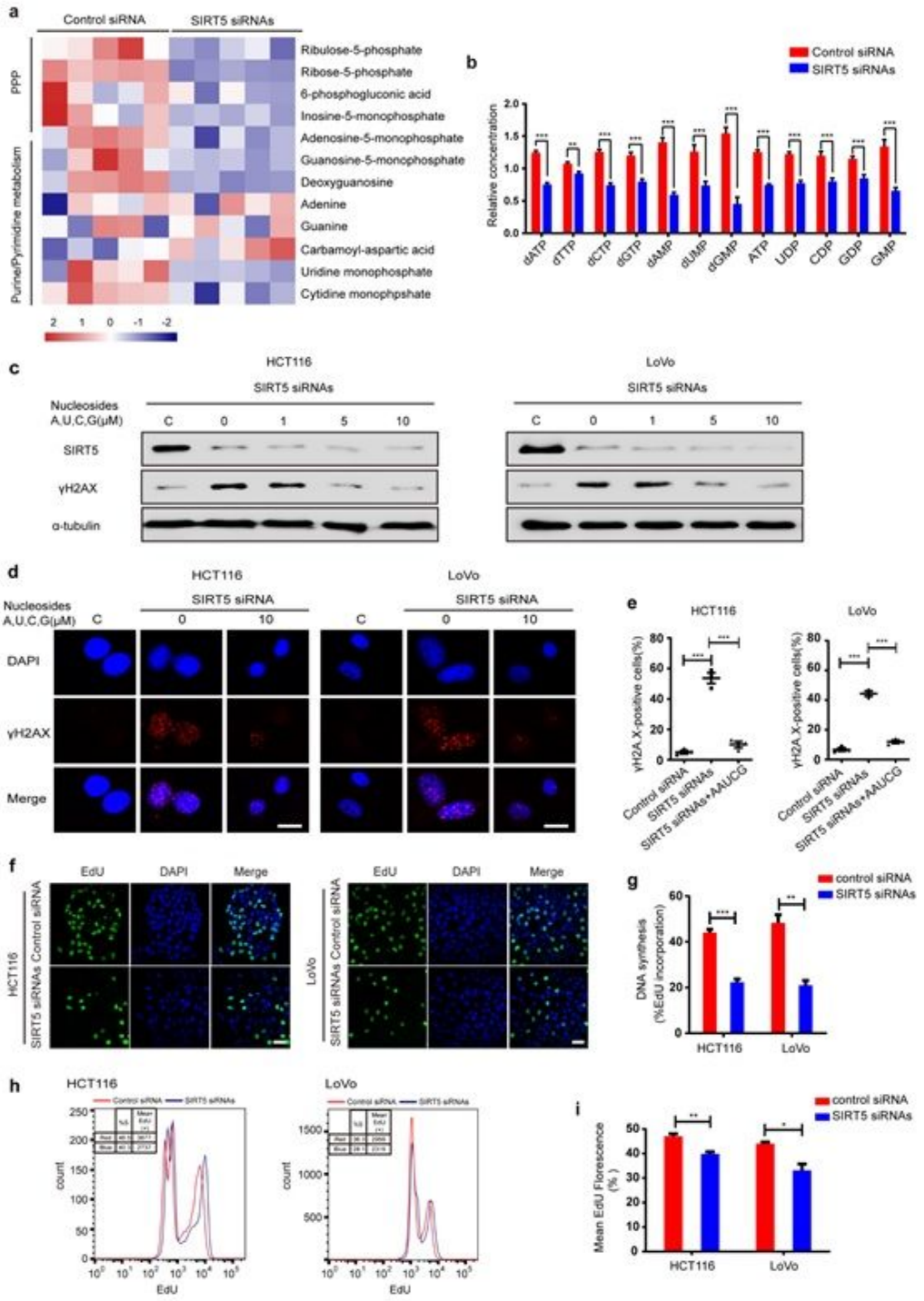

Figure 2

SIRT5 sustained the nucleotide pool by enhancing the synthesis of R5P, to maintain DNA stability. a A Heat map representing significantly different metabolites in PPP and purine/pyrimidine metabolism after the deletion of SIRT5 in HCT116 cells. n = 5. b Targeted metabolomic analysis for nucleotides in HCT116 cells after SIRT5 knockdown. Results are presented as the mean ± SD of five independent samples (**P < 0.01, ***P < 0.001). c-e Exogenous supplementation with nucleotides decreased the levels of γ-H2AX,

induced by silencing SIRT5. Cells were transfected with SIRT5 siRNAs for 48h and cultured at the indicated concentrations with a mixture of four nucleotides for 16h. Immunoblotting (c) and Immunofluorescent staining (d) for γ-H2AX. Quantitation of the γ-H2AX fluorescence intensity (e). f-i Silencing SIRT5 inhibited DNA synthesis in CRC cells. The EdU assay evaluated using Immunofluorescent staining (f) and Flow cytometry (h), is presented. Quantitation of the EdU incorporation rate is shown in a histogram (g, i), representing mean fluorescence intensity of the EdU+ population ± SD of experimental triplicates. Statistical significance was calculated using the two-tailed unpaired t test, *p<0.05, **p<0.01, ***p<0.001.

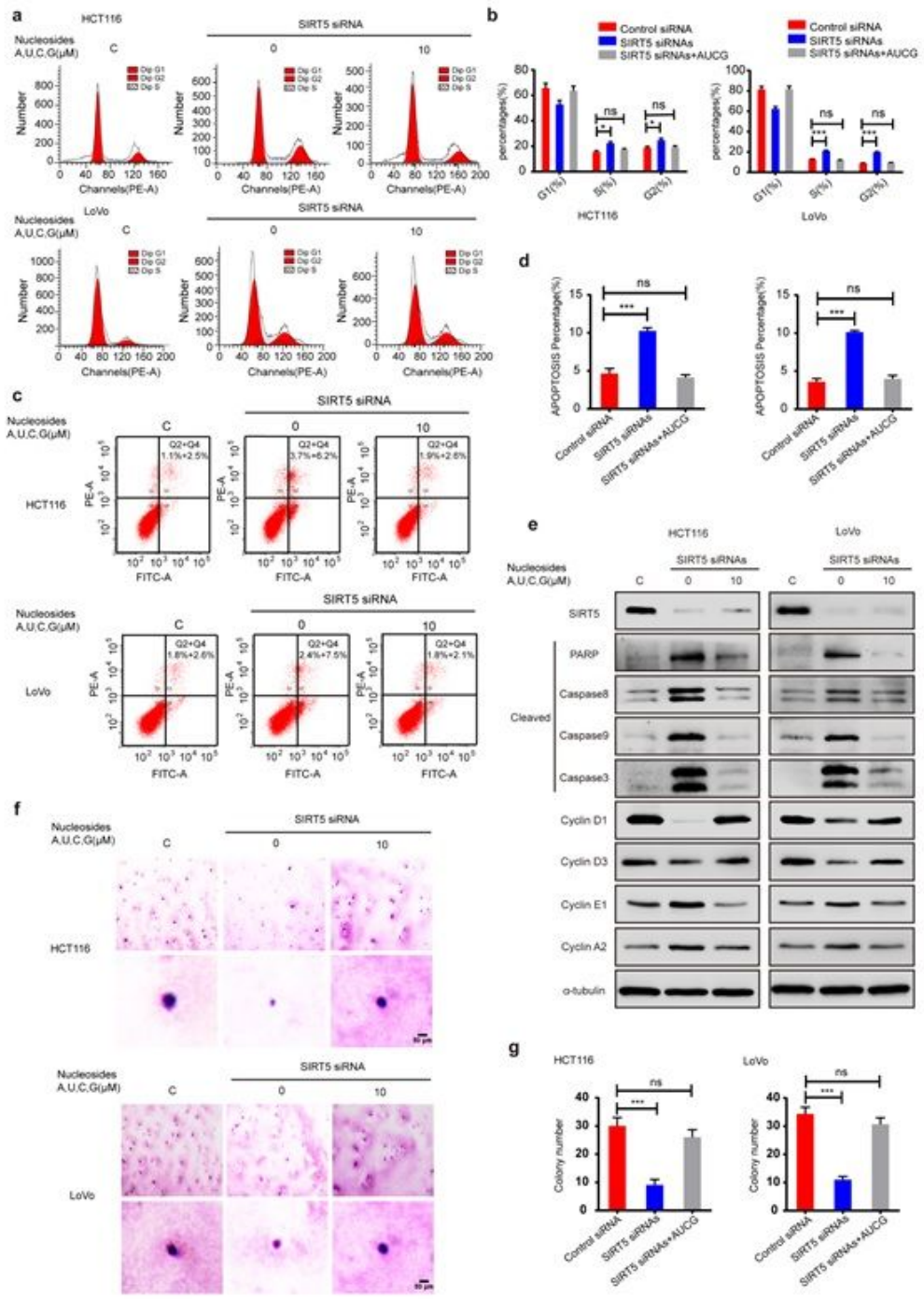

Figure 3

Exogenous supplementation with nucleotides reduced the effects of silencing SIRT5 on the cell cycle, apoptosis and colony formation in CRC cells. a, b Exogenous supplementation with nucleotides reversed the SIRT5 silencing-induced arrest of both the G2/M and S phases (a). The data in a is quantified (b). c, d Exogenous supplementation with nucleotides reversed the SIRT5 knockdown-induced apoptosis (c). Data in c is quantified (d). e Western blotting analysis showed that exogenous supplementation with

nucleotides reversed the levels of apoptosis indicators (the cleaved caspase 8, caspase 9, caspase 3 and PARP) and cell cycle regulators caused by SIRT5-silencing in HCT116 and LoVo cells. f, g Representative images (f) and quantification (g) of using soft agar colony formation after blockage of SIRT5 with or without four nucleotides in the indicated concentrations. Each experiment was performed in triplicate. Scale bar, 50 μm. Data in b, d and g are shown as the mean ± SD. ANOVA with Tukey's test. *p < 0.05,*p < 0.05, ***p < 0.001.

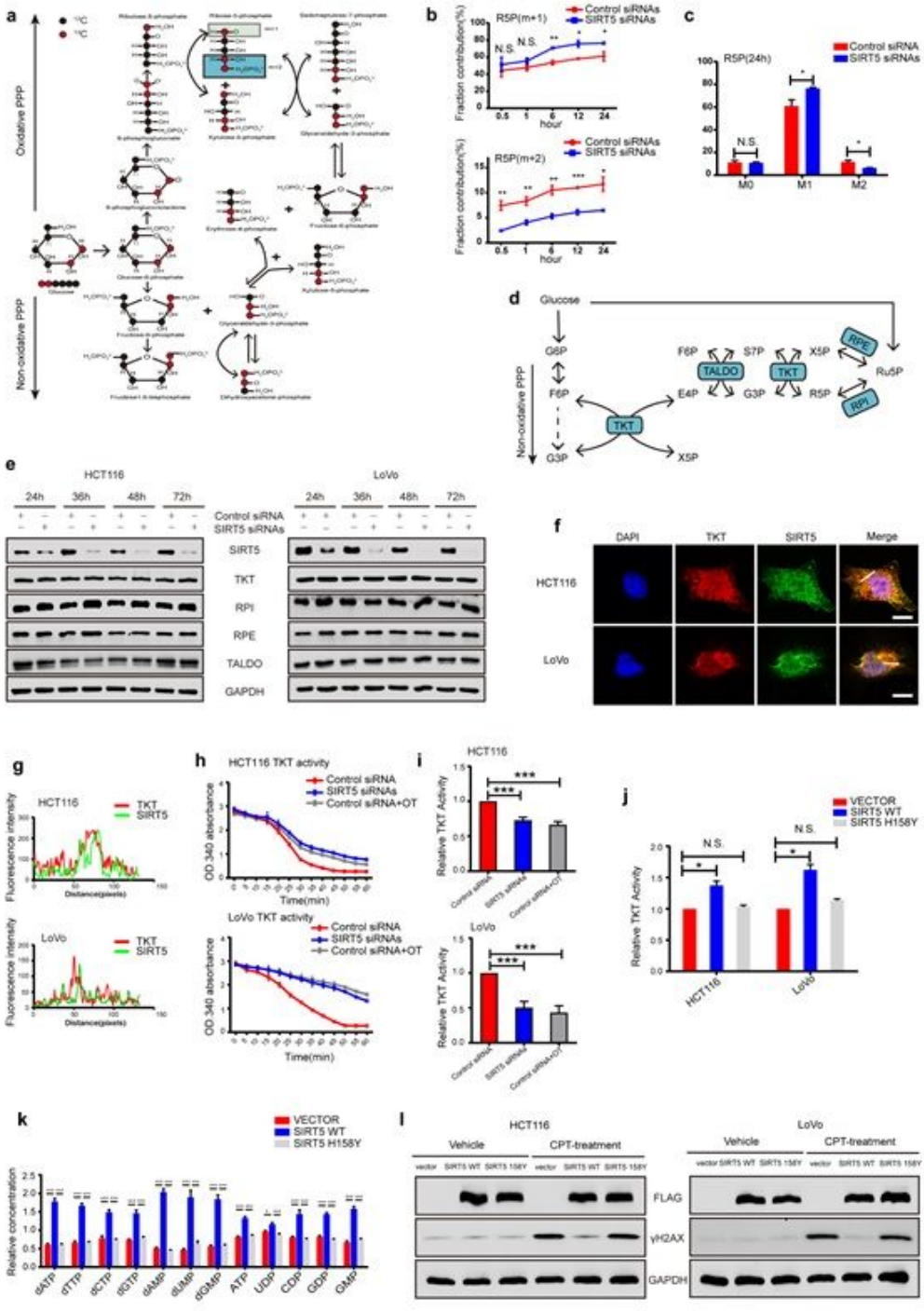

Figure 4

SIRT5 promoted non-oxidative PPP by activating TKT. a [1,2-13C2]glucose was converted to R5P (M+1) through oxidative PPP and R5P (M+2) was generated from non-oxidative PPP. b The ratio of R5P (M+1) to R5P (M+2) from [1,2-13C2]-glucose was determined after SIRT5 knockdown; n = 3. c Quantitative analysis of the R5P sources at 24 h. Data is presented as mean ± squared error (SEM) and the bar indicates the mean. Statistical significance was calculated using the two-tailed unpaired t test. d A schematic model of the key enzymes involved in non-oxidative PPP in cells. e Expression of TKT, RPI, PPE and TALDO after depletion of SIRT5. f, g Immunofluorescent staining for SIRT5 (in green) and TKT (in red) respectively, the yellow in the merged magnified images indicates the co-localization (f). Scale bars indicate 5μm. Fluorescence intensity of SIRT5 (green line) and TKT (red line) traced along the white line in CRC cells using the line profiling function of the ImageJ software (g). h, i TKT enzyme activity was determined following SIRT5 knockdown in HCT116 and LoVo cells (h).Quantification of TKT activity is shown in a histogram (i, n = 3). The TKT inhibitor, Oxythiamine (OT; 20 μM) was used as a positive control. j TKT enzyme activity was determined in HCT116 and LoVo cells stably expressing the control vector, SIRT5 WT or SIRT5 H158Y. Quantification of TKT activity (n=3). k Targeted metabolomic analysis for nucleotide levels in HCT116 cells stably expressing the control vector, SIRT5 WT and SIRT5 H158Y. l Immunoblotting of γ-H2AX in HCT116 and LoVo cells stably expressing the control vector, SIRT5 WT and SIRT5 H158Y, cultured with or without CPT. Data in i, j and k are shown as the mean ± SD of three independent samples. ANOVA and the Tukey’s test were used. ns, not significant in the indicated comparison, *$p < 0.05$, **$p < 0.01$, ***$p < 0.001$.

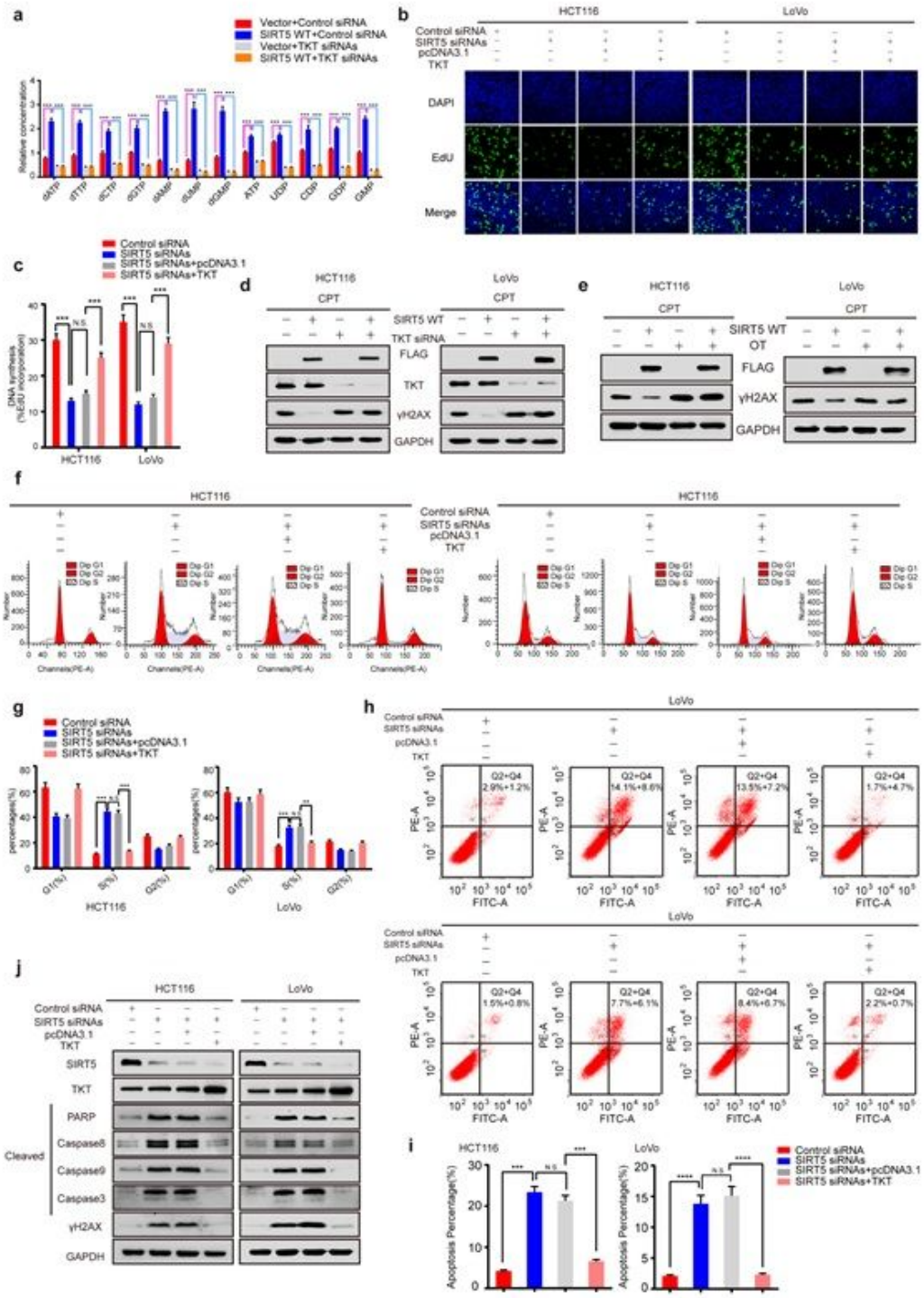

Figure 5

TKT played a role in the SIRT5 knockdown-induced presence of an insufficient nucleotide pool and subsequent DNA damage in CRC Cells. a Targeted metabolomic analysis of nucleotide levels in HCT116 cells stably expressing the control vector and SIRT5 WT treated with the TKT-siRNA. b, c The EdU assay of HCT 116 and LoVo cells showed that overexpression of TKT reversed the decrease in DNA synthesis induced by silencing SIRT5 (b). Quantification of the EdU incorporation rate in CRC cells (c). d, e

Immunoblotting of γ-H2AX in HCT116 and LoVo cells stably expressing the control vector and SIRT5 WT treated with the TKT-siRNA (d) or OT (20 μM, e). 1mm CPT was used as a DNA-damaging agent. f-i Flow cytometry was used to detect the effect of overexpressing TKT on the cell cycle (f) and apoptosis (h) in CRC cells where SIRT5 was silenced. The data in f is quantified (g). Data in h is quantified (i). (J) Western blots showing that overexpression of TKT inhibited the apoptosis induced by SIRT5 knockdown. Data in c, g and i are shown as the mean ± SD of three independent samples. ANOVA and the Tukey's test were used.

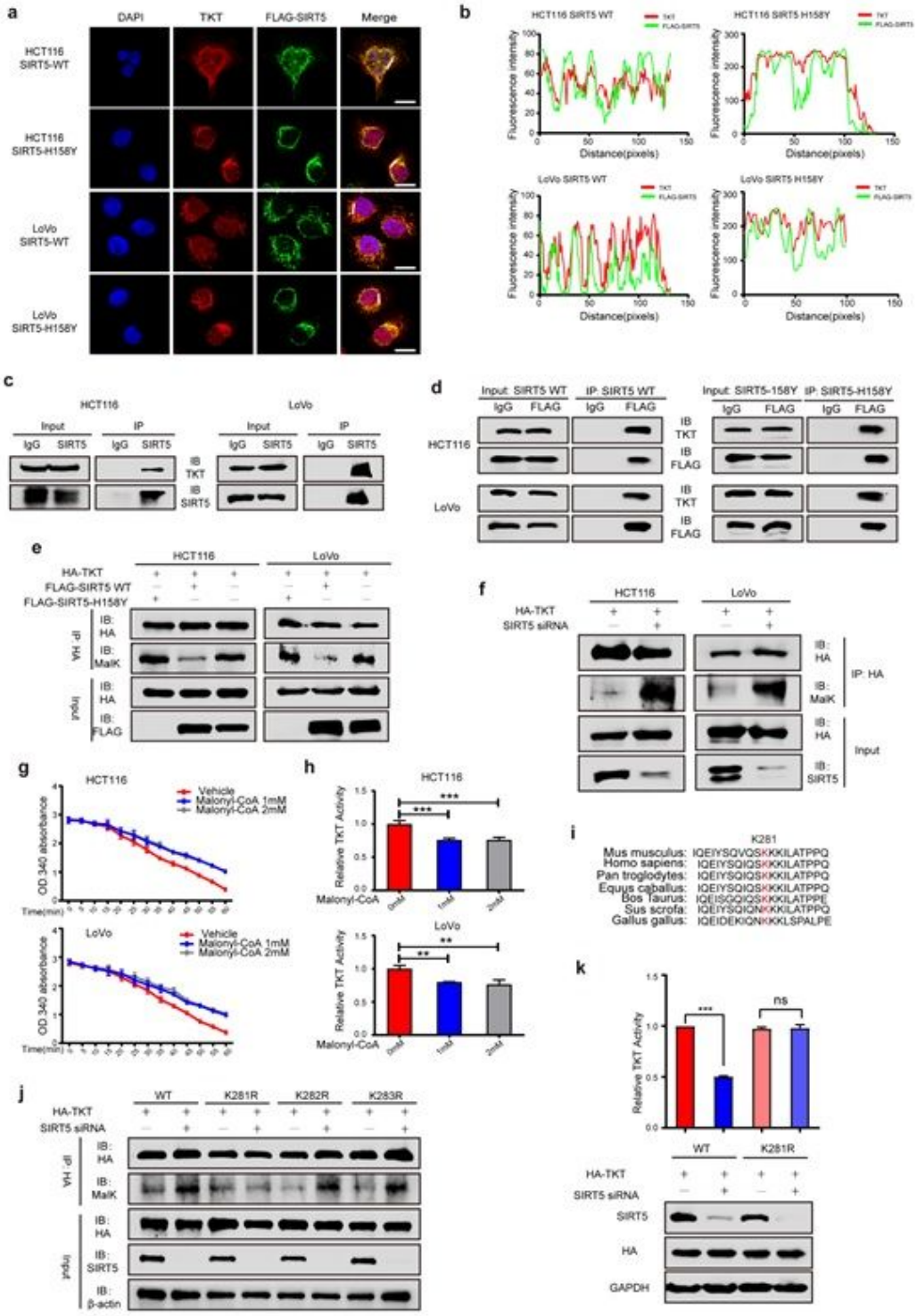

Figure 6

SIRT5 activated TKT by mediating its demalonylation. a, b Immunofluorescent staining results for FLAG-SIRT5 WT/H158Y (in green) and TKT (in red). The yellow in the merged magnified images indicates the co-localization. Scale bars indicate 10μm (a). The fluorescence intensity of FLAG-SIRT5 WT/H158Y (green line) and TKT (red line) traced along the white line in HCT116 and LoVo cells using the line profiling function of the ImageJ software (b). c The interaction between endogenous SIRT5 and TKT in HCT116 and LoVo cells. d FLAG-SIRT5 WT/H158Y were immunoprecipitated with the anti-FLAG antibody, followed by western blotting using an anti-TKT antibody in HCT116 and LoVo cells. e The malonylation (Malk) levels of exogenous TKT in HCT116 and LoVo cells expressing the control vector, SIRT5 WT and SIRT5 H158Y. f The malonylation (Malk) levels of exogenous TKT in HCT116 and LoVo cells after SIRT5 knockdown. g, h The levels of TKT activity using different concentrations of Malonyl-CoA (0, 1 and 2 mM) measured at 37 °C for 60 min in HCT116 and LoVo cells overexpressing TKT (g). HA-tagged TKT proteins were purified using IP. Quantification of TKT activity (h). i The K281 of TKT is evolutionarily conserved across different species. These sequences of TKT from humans to Gallus gallus were aligned. j HA-tagged TKT WT/K281R/K282R/K283R mutants were transfected into HCT116 followed by treatment with SIRT5 siRNAs. TKT was immunoprecipitated and the levels of MalK determined. k HCT116 cells expressing TKT WT and K281R mutants, with or without SIRT5 siRNAs. TKT activity was measured and normalized against the protein levels. The results in (h, k) are the mean ± SD of three independent experiments. p values were calculated through ANOVA and the Tukey's test. *$p < 0.05$, **$p < 0.01$, ***$p < 0.001$, ns = not significant in the indicated comparison.

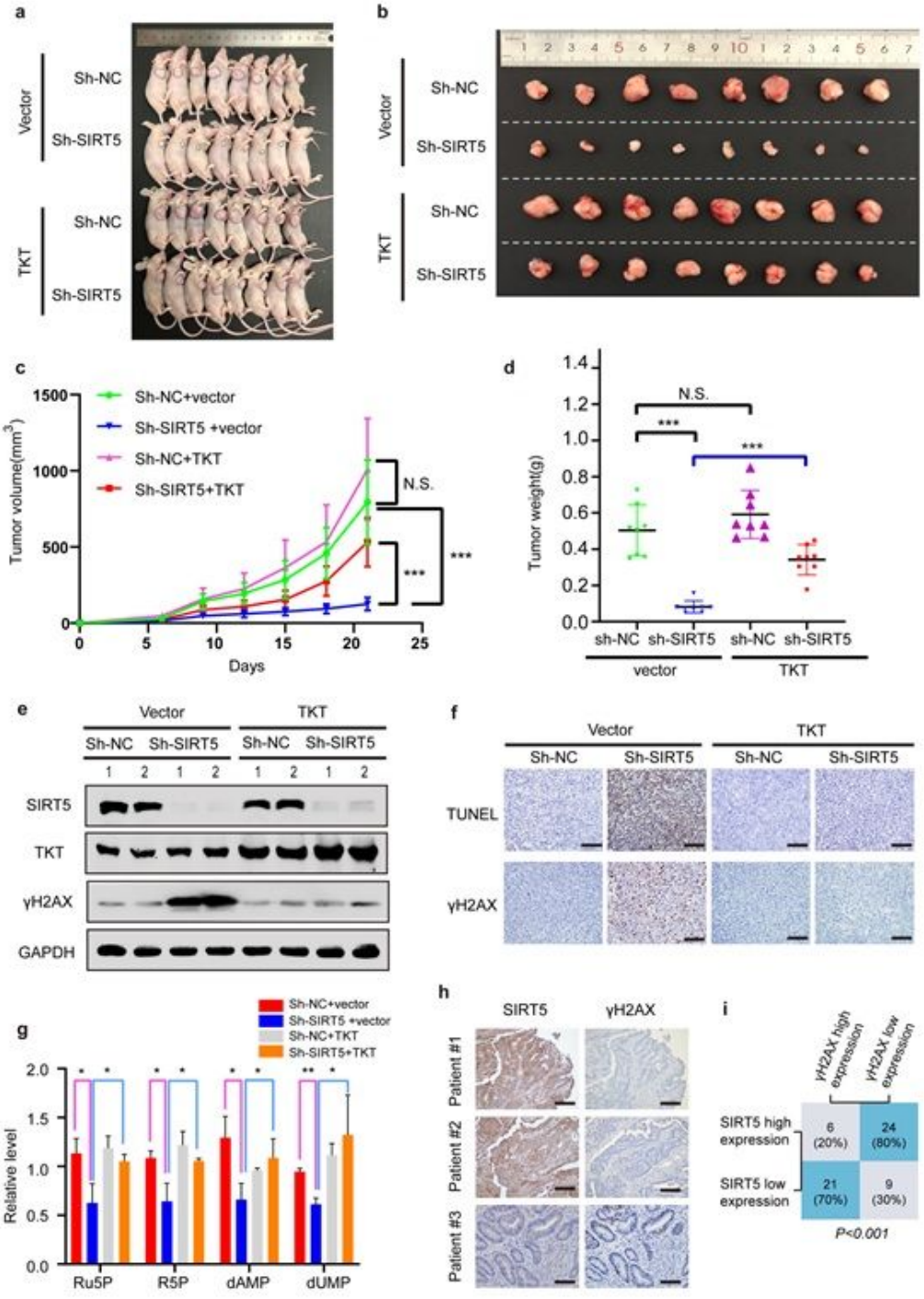

Figure 7

The function of TKT in SIRT5-mediated tumorigenesis in vivo. a-d Tumors from different groups were dissected and photographed (a, b), and the volumes and weights of the tumors were measured (c, d). Data is presented as the mean ± SD. (*p < 0.05, ***p < 0.001). e Immunoblotting of SIRT5, TKT and γ-H2AX proteins in xenografts tumor tissues under different treatments. f Representative TUNEL and γ-H2AX stains from xenograft tumors at day 21. Scale bars, 50 μm. g The levels of R5P and nucleotides in

tumor lysates derived from xenografts. Data is presented as the mean ± SD. (*P < 0.05, **P < 0.01). h Representative immunohistochemistry images of the SIRT5 (left) and γ-H2AX (right) proteins in CRC tissues. i Statistical analysis of SIRT5 and γ-H2AX staining in 60 CRC tissues. Statistical significance was assessed using the Chi-square test. *p < 0.05, **p < 0.01, ***p < 0.001, ns = not significant in the indicated comparison.

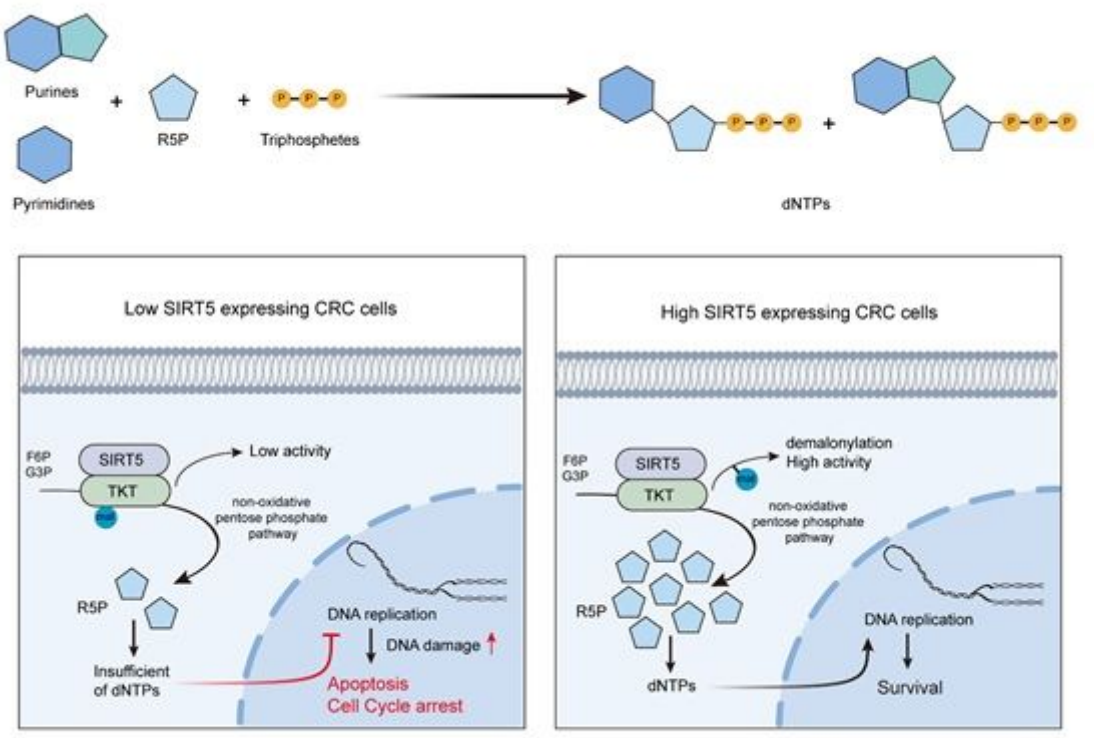

Figure 8

Schematic model showing that SIRT5 promotes the non-oxidative PPP by interacting with TKT, resulting to the demalonylation and activation of TKT. This maintains the levels of intracellular R5P and dNTPs, thus supporting the survival of CRC cells.

Supplementary Files

This is a list of supplementary files associated with this preprint. Click to download.

- supplementfigure20210225.docx